Energy Conversion and Management: X 23 (2024) 100663

Contents lists available at ScienceDirect

Energy Conversion and Management: X

journal homepage: www.sciencedirect.com/journal/energy-conversion-and-management-x

A MATLAB script and a methodology for the powertrain design of a fuel cells-battery hybrid electric supercar

Martino Diana, Lorenzo Martoccia *, Stefano Fontanesi, Valerio Mangeruga, Alessandro d'Adamo

Dipartimento di Ingegneria "Enzo Ferrari", Università degli Studi di Modena e Reggio Emilia, Modena, Italy

ARTICLE INFO

Keywords:
Fuel cell powertrain
Hydrogen supercar

ABSTRACT

The urgency to decarbonize the transportation sector covers all kinds of vehicles, here included high-performance competition vehicles. Among the technologies able to guarantee zero emissions during the use phase, fuel cells (FCs) and energy storage systems (ESS), e.g. batteries, offer a great and still largely underexplored potential for complementary and synergic use in hybrid powertrains. Vehicles based on such technologies are cells-battery hybrid electric vehicles (FCHEV), and a niche of these are electric supercars (FCHES). In this context, the degrees of freedom of hybrid powertrains design and the different requirements of FCs and batteries frame the highly complex task of defining a clear and objective methodology to identify an optimal ratio among FC-battery power sources, whose lack jeopardizes a rigorous decision process as well as a general consensus and leads to the acceptance of sub-optimal solutions.

In this study an energy/power-based methodology is developed in MATLAB environment considering the longitudinal vehicle dynamics of a typical high-performance parallel FCHES, using telemetry data from a real racetrack as common target for all the evaluated powertrain candidates and using realistic mass values. Under the constraint of equal performance (i.e., equal lap time), several FC-battery parallel hybrid powertrains are numerically evaluated with varying relative energy, power, weight, and under different regenerative braking levels. The set of obtained results allows to draw an objective rightsizing on the FC-battery power share and on the required energy capacity for a parallel FCHEV, as well as mass, hydrogen consumption, etc. The presented methodology offers a general use workflow applicable to any category of vehicles, supporting the engineering of hybrid FC-battery high-performance propulsion systems. The developed code will be made available upon request under the FAIR (Findable, Accessible, Interoperable, Reusable) guidelines.

1. Introduction

The urgency to decarbonize the transportation sector has led to the emergence of hybrid powertrains in the past decades, combining the complementarity of conventional internal combustion engines (ICEs) with battery-powered electric motors (EMs), allowing state-of-the-art reduction in fuel consumption thanks to the possibility to operate the ICE/EM at their maximum efficiency and to the possibility to recover part of the braking energy to recharge the battery (regenerative braking). However, this has come at the cost of more expensive and complex powertrains, due to the coexistence of multiple power sources and the need to define control logics for their synergic operation. In the quest for powertrain electrification, fully electric powertrains have recently emerged in the form of Battery Electric Vehicles (BEVs) and Fuel Cells Electric Vehicles (FCEVs), the former solely relying on a battery pack fulfilling the entire energy and power needs of the vehicle, whereas the latter separating the energy storage in the fuel (e.g., hydrogen) tank from the power generator (the energy converter, i.e. the fuel cell) [1,2]. In mobility applications, Polymeric Electrolyte Membrane Fuel Cells (PEMFCs) have emerged as the candidate cell type, given the absence of corrosive liquids, the high power density, and the rapid response; however, fuel cells are inherently not suitable to highly rapid load transients due to accelerated membrane and catalyst degradation and to the risk of reactants starvation at electrodes. This has created the need for an auxiliary power source (e.g. a low-to-medium capacity battery) for peak power demands, leading to Fuel Cell-battery Hybrid Electric Vehicles (FCHEV) [3].

In a generic hybrid powertrain, the general layout (e.g. series/

* Corresponding author at: Dipartimento di Ingegneria "Enzo Ferrari", Università degli Studi di Modena e Reggio Emilia, Via P. Vivarelli 10, 41125 Modena, Italy.
E-mail address: lorenzo.martoccia@unimore.it (L. Martoccia).

https://doi.org/10.1016/j.ecmx.2024.100663
Received 6 May 2024; Received in revised form 5 July 2024; Accepted 6 July 2024
Available online 7 July 2024

parallel, etc.) as well as the logical rules for the power share between the multiple power sources are crucial design choices, determining a cascade of consequences regarding the components design (e.g. auxiliary systems, cooling circuit design, etc.). In this fundamental design stage, several methods and tools were created to support the powertrain development as well as to compare alternative solutions, especially when the introduction of innovative technologies prevented a carry-over of pre-existing concepts. In this context, the ADVISOR [4–6] code from the National Renewable Energy Laboratory (NREL) was the first publicly available tool to investigate model-based powertrain comparisons [7,8], supported by several validation studies carried out on commercially available hybrid light-duty vehicles [9,10]. In [11] Huang et al. used embedded ADVISOR models to study the hybrid ratio (i.e., FC/battery power share) of a FCEV, although the generality of the identified value (0.59) was not discussed. Feng et al. [12] studied a virtual FC-battery hybrid powertrain for a bus on several driving cycles, identifying the respective power levels to 70 and 50 kW. Similar studies were conducted by Cipollone et al. [13] and Di Battista et al. [14], who introduced a power-based methodology to size the powertrain of a FCHEV, focusing on a research vehicle and on the re-design of a BEV architecture to maximize the driving range, respectively. Carignano et al. [15] presented an accurate model-based description of the Toyota Mirai FC-battery hybrid powertrain, still being able to consider a FC rated power of 80 kW based on duty cycle assumptions and corroborating the design choices of the existing model. Di Ilio et al. [16] designed a parallel hybrid fuel cell-battery powertrain for a heavy-duty yard truck for port logistics, sizing the fuel cell on the mean power requested by the duty cycle and choosing a battery able to provide the remaining power contribution to the maximum requested power. However, under the typical constraint of state of charge recovery (i.e., the ESS state of charge at the end of cycle must be identical to the initial one), and even in the hypothesis of a steady-state FC operation at the target power, the incompleteness of regenerative braking and the efficiencies associated with battery charging/discharging process invalidate the choice of its target power value as the exact mean value of the power profile. Hence, an iterative procedure needs to be developed, as discussed in Cipollone et al. and Di Battista et al. [13,14], which must include the powertrain mass variation associated to the iteration on power/energy for FC/ESS, respectively. More recently, Jouda et al. [17] proposed a comparison of learning-based methodologies to optimize the fuel economy of a hybrid fuel cell vehicle, although they dealt with an existing FCHEV and the control strategy was the object of the study, hence not addressing the issue of rightsizing the baseline powertrain. Li et al. [18] proposed an adaptive Energy Management System (EMS) method for FCHEV, again addressing the issue of identifying the best control strategy. Hu et al. [19] presented an EMS study dealing both with fuel economy and with durability of fuel cell and battery combining deep reinforcement learning (DRL) and Pontryagin's minimum principle (PMP), and Fu et al. [20] applied an adaptive random forest (ARF) algorithm for an online EMS for a generic FCHEV. The mentioned studies make an advanced use of machine learning (ML) models to optimize EMS, rather than to rightsize the powertrain components, still showing that despite the availability of useful tools to compare alternative powertrains, still several assumptions are used to define key input data (e.g., the FC power equal to the mean duty cycle power) in the design of a hybrid FC-battery powertrain. In case such inputs are not available, or when designing a brand-new innovative powertrain, the lack of a general-use methodology leads to a non-rigorous decision process or to a trial-and-error approach. Hence, the knowledge gap that is identified is the need for creation of an objective methodology to design a hybrid fuel cell-battery powertrain to support its fundamental choices, e.g. the power share between the fuel cell and the auxiliary power source, as well as the energy capacity of this last. To this aim, a power- and energy-based general methodology is devised in this study for a parallel-type FCHEV powertrain, whose generality applies to all kind of vehicles and duty cycles. The study is conducted in MATLAB environment, and the developed code will be made fully accessible upon request under the FAIR (Findable, Accessible, Interoperable, Reusable) indications. For demonstration purposes, the methodology is applied to a high-performance supercar (FCHES) on a racetrack driving cycle, and two power share strategies (FC- and ESS-dominant, respectively) are tested, with and without regenerative braking. This vehicle choice well represents a case where hybrid FC-battery propulsion is unusual to date, and where the upcoming decarbonization targets will require brand-new propulsion architectures to be devised. Therefore, this study exemplifies the early stage of a brand-new innovative powertrain development. The results show that for all cases well-defined ranges of ESS capacity and FC power can be identified as optimal, hence indicating a rightsizing approach for both power/energy sources. This is considered a decisive support tool in guiding the designer in the careful selection of components, and the model generality is considered a key enabler for the development of decarbonized powertrains in all the mobility sectors.

2. Methodology

2.1. Model equations

The development of an innovative powertrain architecture requires a method to predict the vehicle performance and driving range. From the perspective of a powertrain designer, the objective is to formulate a mathematical model of the vehicle, enabling parametric evaluations associated with variations in fundamental design parameters such as mass, power, and stored energy, which are of interest for all the powertrain architectures. In case of a hybrid powertrain, a key design choice is the definition of the power share between the multiple power sources. All vehicles must produce a tractive effort to satisfy the power demand of the driver, be it for a homologation test or to achieve a performance target. This force propels the vehicle, and it is transmitted to the ground by the drive wheels. It can be calculated using a simple model for the vehicle longitudinal dynamics, here reported for completeness. Considering a vehicle of mass m, with a velocity v and a road with a slope of angle φ, the resistances that must be overcome are associated to the rolling resistance, to the aerodynamic drag, to the resistance caused by the component of the vehicle's weight acting down the slope, resulting in the vehicle longitudinal acceleration under a given tractive power. The rolling resistance (F_{rr}, Eq. (1)) is mainly caused by the hysteresis losses in the tires, and it is approximated as independent of the vehicle speed and only a function of its weight and of the coefficient of rolling resistance (μ_{rr}), although velocity-dependent formulations could be introduced for further detail [1].

$$F_{rr} = \mu_{rr} mg \tag{1}$$

The aerodynamic drag (F_{ad}, Eq. (2)) depends on the vehicle frontal area (A), on the drag coefficient related to aerodynamic design (C_d), on the air density (ρ), and on the vehicle speed.

$$F_{ad} = \rho A C_d v^2 \tag{2}$$

The hill climbing force (F_{hc}) is the force necessary to overcome a slope, calculated as in Eq. (3):

$$F_{hc} = mg\sin\varphi \tag{3}$$

Finally, during the acceleration transients, a force is needed to modify the vehicle speed. From Newton's second law, the linear acceleration of the vehicle (F_{la}) is calculated as in Eq. (4). Ignoring the contribution related to the rotational acceleration (i.e., the force associated to angular acceleration of the rotating parts), a reasonable approximation can be adopted by increasing the mass by 5 % in Eq. (4), following the assumption in [2].

$$F_{la} = ma \tag{4}$$

The total tractive effort (F_{te}) is the algebraic sum of all the previously described terms, as in Eq. (5), and the required tractive power (P_{te}) to obtain a prescribed speed and distance profile is calculated as in Eq. (6):

$$F_{te} = F_{rr} + F_{ad} + F_{hc} + F_{la} \tag{5}$$

$$P_{te} = F_{te} v \tag{6}$$

In order to relate the tractive power to that needed by the electric motor, the powertrain efficiencies are included in the model. Considering an electric vehicle, the efficiency of the gear system (η_g) is generally assumed to be constant, as there is only one gear. The efficiencies of the motor and its controller (inverter) are typically bundled (η_{mot}), given the practical convenience in measuring the efficiency of the entire system. The efficiencies of the motor, controller, and gear system imply that the electrical power demanded by the motor ($P_{mot_{in}}$, Eq. (7)) exceeds the mechanical motor's power ($P_{mot_{out}}$), which is higher than the traction power (P_{te}) according to Eq. (8):

$$P_{mot_{in}} = \frac{P_{mot_{out}}}{\eta_{mot}} \tag{7}$$

$$P_{mot_{out}} = \frac{P_{te}}{\eta_g} \tag{8}$$

During the deceleration phase, the electric motor can be used to slow the vehicle and the efficiencies operates in the opposite direction. Therefore, less power is obtained from the motor, as in Eq. (9):

$$P_{mot_{in}} = P_{mot_{out}} \eta_{mot} \tag{9}$$

Concerning the energy storage system (ESS), the same principles regarding efficiency can be applied as those described for the motor. In this study, the concept of a generic ESS is used for maximum generality, thus being applicable both to rechargeable batteries and supercapacitors. Therefore, when the ESS is providing power (P_{ess}) to the motor Eq. (10) is used, whereas when the motor operates as a regenerative device Eq. (11) is used.

$$P_{ess} = \frac{P_{te}}{\eta_{ess}} \tag{10}$$

$$P_{ess} = P_{te} \eta_{ess} \tag{11}$$

Throughout the study, a positive power value indicates that it is delivered from the power source, i.e. the powertrain (FC or ESS, or both) is supplying power, whereas a negative power denotes braking or ESS recharging. This last contribution originates either from the fuel cell system or via regenerative braking.

Considering the overall efficiency η_m (including motor and drivetrain efficiencies), in case of a positive tractive power (P_{te}) Eq. (12) is used, with the opposite sign Eq. (13) is used.

$$P_m = \frac{P_{te}}{\eta_m} \tag{12}$$

$$P_m = P_{te} \eta_m \tag{13}$$

Finally, during the braking phase a regenerative power flow (P_{rb}) is calculated as in Eq. (14), with r_b being a defined coefficient ranging from 0 (no regenerative braking recovery) to 1 (complete regenerative braking recovery). The remaining power is dissipated via mechanical braking.

$$P_{rb} = r_b P_{te} \tag{14}$$

2.2. Drive cycle

As a reference drive cycle for a FCHEV, the telemetry of the Noao car, a hybrid electric racing car developed by the Association des Entreprises Pole de la Performance Nevers Magny-Cours [21] is used. The published data consist of velocity and time profiles which have been recorded in the international circuit of Magny-Cours (Fig. 1 [21]). In this study, the original speed telemetry data is multiplied by a factor of 1.5 to represent the performance levels of a typical supercar (Fig. 2). Starting from the telemetry data, the required power to realize the speed and distance profile is reported in Fig. 3.

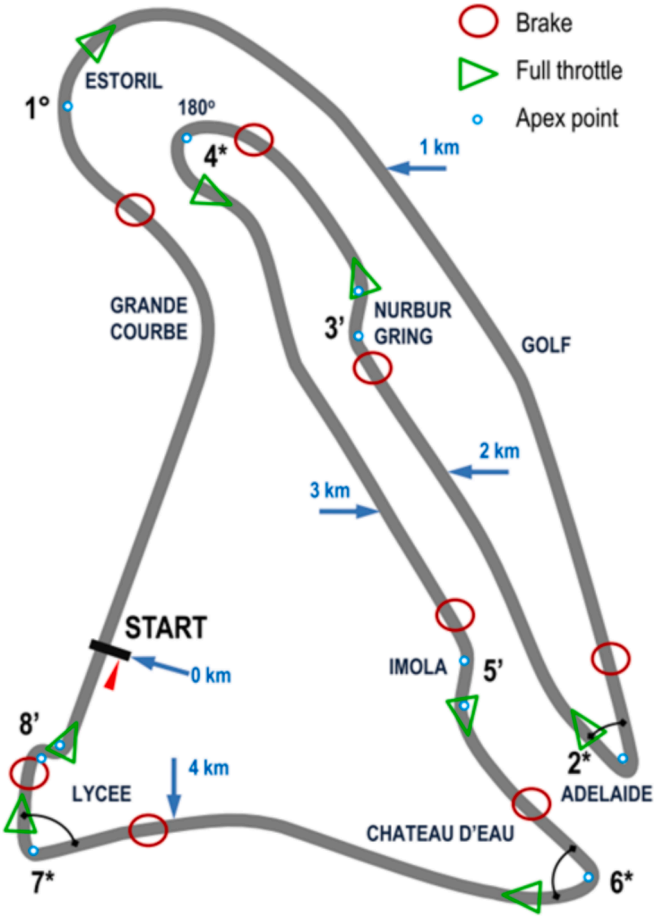

Fig. 1. Map of the Magny-Cours circuit, from [21].

2.3. Power split model

The idea underlying this study is to devise a comprehensive yet generic methodology to address the power split in the architecture of fuel cell-hybrid electric vehicles, here demonstrated on a supercar case (FCHES). Starting from the fundamental vehicle model described in Section 2.1 and the duty cycle in Section 2.2, still a degree of variability remains in infinite combinations to distribute the power between the two sources, unless additional constraints and specifications are added. The main objective of the presented methodology is to determine fundamental design aspects, such as the power output of the FC and the optimal size of the ESS under equal performance, including their weight impact on the vehicle mass and on the hydrogen consumption and storage requirements, and not on optimizing the control strategy. For advanced optimization of the power control strategy the reader is referred to specific sources [22], but the aim of the present study is to discuss a universal methodology for FC/ESS sizing for a generic vehicle and duty cycle. In this context, the study does not delve into the detailed characteristics of the FC or of the ESS (e.g., in case of a rechargeable battery the type of cell, number of cells, etc.), but rather addresses the topic from the general perspective of power repartition between FC/ESS

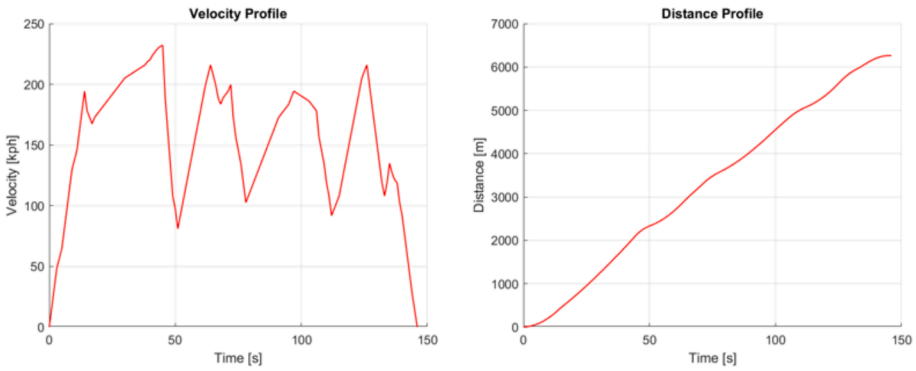

Fig. 2. Velocity and distance profiles of a single lap of the Magny-Cours circuit, modified from [21] for the present study.

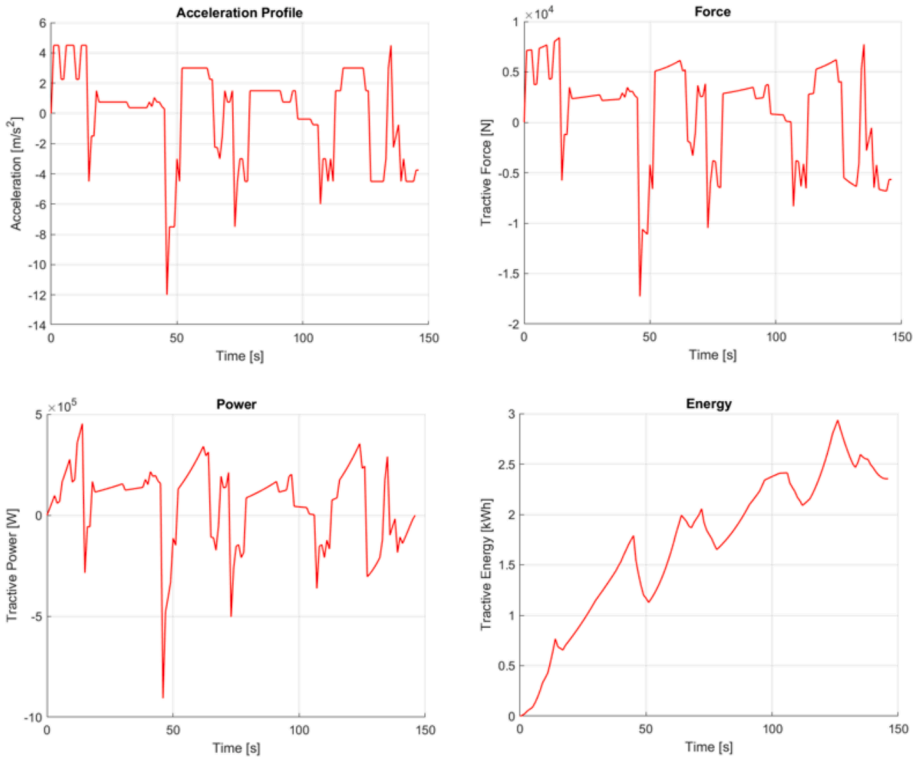

Fig. 3. Acceleration [m*s^{-2}], tractive force [N], power [W] and energy [kWh] profiles extrapolated from the telemetry data.

to deliver a specific performance, which will be finally differentiated based on criteria such as the specific hydrogen consumption. These are the fundamental design data needed to guide the identification of performance targets for both the FC and ESS, be it for internal development as well as to select them from supplier's datasheets.

The study is conducted in the MATLAB environment, developing an in-house code using the speed profile of the designated driving cycle as a common boundary condition (mission) for all the investigated solutions. Therefore, all the evaluated powertrains deliver an identical performance (i.e., lap time), although largely differing in the respective masses of the FC/ESS. An iterative procedure is incorporated to introduce a constraint on the State of Charge (SOC) recovery of the ESS, i.e. the end-of-mission SOC value must be within a prescribed tolerance from the begin-of-mission SOC value. Once convergence is reached, the model indicates a target power that the FC must deliver to the ESS. The described process is reiterated for increasing ESS sizes, each characterized by an increment in the energy content (measured in kWh). After each iteration, the procedure incorporates the update of the FC powertrain mass, determined by the maximum power to be delivered throughout the drive cycle, and the adjustment of the FC and ESS mass. The data pertaining the variability in the mass of the FC (comprising the mass of the fuel cell stack and all necessary auxiliaries for complete functionality) are derived from publicly available datasheets of commercial fuel cells (Ballard, Symbio, etc.) [23], whereas for the ESS a dedicated database on Li-ion battery packs is employed containing information on the mass of the battery cell and the entire package (including the shell, cables, etc.) [24]. For the scope of the powertrain sizing, linear regressions are assumed for both FC and ESS sizing on power and energy, respectively, although more refined non-linear functions can be used. The objective is to compare several powertrain architectures on an equal performance basis, necessarily requiring different output power from FC/ESS and resulting in associated mass variations; the adopted iterative process allows to discern the implications of these variables on the vehicle's performance, finally focus on fuel consumption.

With regard to the ESS, the model introduces assumptions pertaining to the maximum power obtainable or rechargeable. Specifically, the limitation is imposed on the maximum C-rate, defined as the maximum

Table 1
SOC values of the power split optimization model.

Power Split Strategies	Parameter	Value
V1 – V2	SOC_{init}	0.9
	SOC_{min}	0.1
	SOC_{max}	1.0
	SOC_{on}	0.2
	SOC_{off}	0.95
V2	SOC_{REx_low}	0.4
	SOC_{REx_up}	0.95

current that the ESS can provide over determined period [2,25]. A maximum limit of C50 is chosen, aligning with the requirements for an electric supercar model.

2.4. Power split strategies

In the perspective of the parallel hybrid powertrain operation, two power distribution strategies have been devised for the FC and the ESS to demonstrate the methodology, hereafter named V1 (*Dynamic*) and V2 (*Range Extender – REx*) strategy. The parameters chosen to discern the different power values are the sign of the tractive power (P_{te}) and the state of charge (SOC) of the ESS.

The V1 strategy imposes a high priority for power delivery on the FC, which is the main power source to follow the power requested by the driving cycle, explaining the *Dynamic* name. For this purpose, specific values of SOC (SOC_{on}, SOC_{off}) are defined and reported in Table 1. The ESS is required to assist the FC in satisfying a portion of the power demanded by the load, within the limit imposed by the assumed C-rate. In Fig. 4 the power levels that are delineated in the code to optimize the power split for the V1 strategy are reported. Primarily, the system's behaviour is dictated by assessing the power requested (P_{mot}). Subsequently, the SOC is examined to determine the magnitude of power that each power source must deliver, attributing to the FC the dominant role in the power supply for the V1 strategy. Additionally, two different levels of power required from the fuel cell (P_{idle},P_{target}, with $P_{idle} < P_{target}$) are defined in order to restore the SOC value in braking conditions and in ESS low-power scenarios.

An alternative scenario is depicted with the V2 strategy, reported in Fig. 5. In this scenario, the ESS is the dominant power source, with the FC serving as ESS recharger to recover the specified initial SOC condition, explaining the *Range Extender – REx* name. For this strategy two values of the SOC are specified in Table 1: when the upper limit (SOC_{REx_up}) is reached, the ESS operates in high power assistance mode (H-PAM), and the power split prescribes the ESS discharge until the lower SOC limit (SOC_{REx_low}) is attained. At this point, the ESS operates in low power assistance mode (L-PAM), and the power split modifies to minimize the power demanded from the ESS, thus facilitating a sufficient recharge of the SOC by the FC and the regenerative braking, if present. Consequently, in L-PAM mode the ESS predominantly recharges until

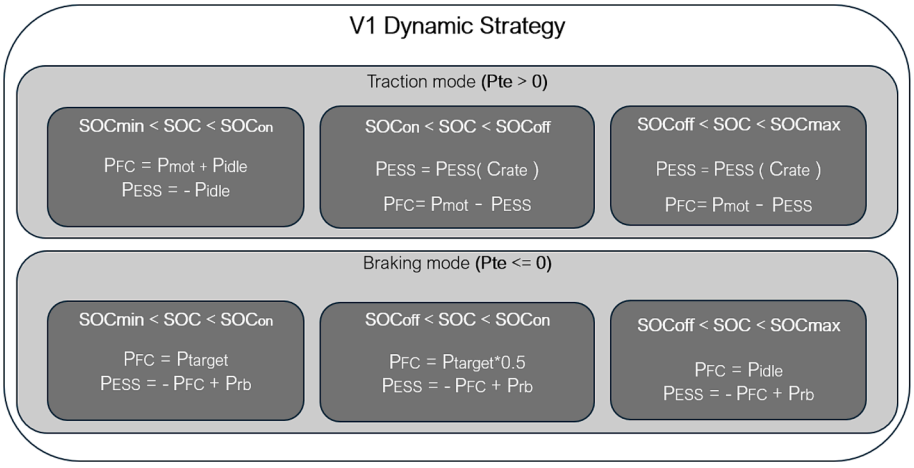

Fig. 4. Synthetic map of the V1 strategy (*Dynamic*).

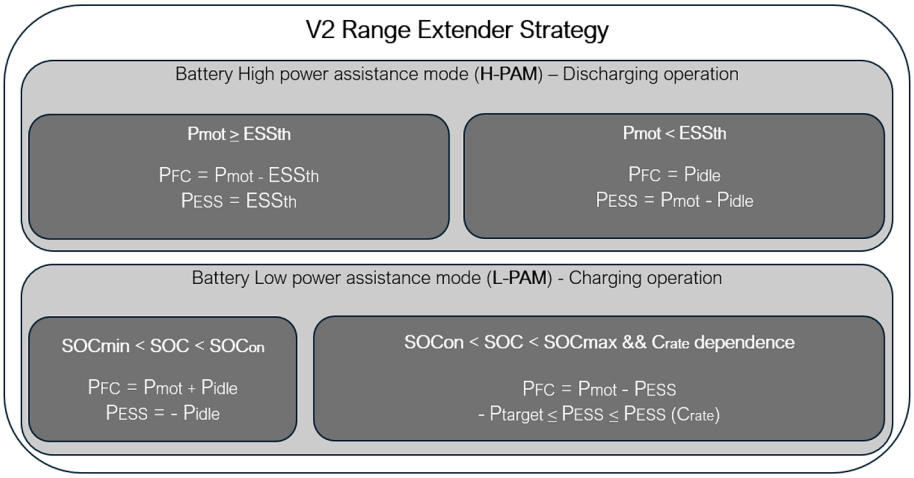

Fig. 5. Synthetic map of the V2 strategy (*REx*).

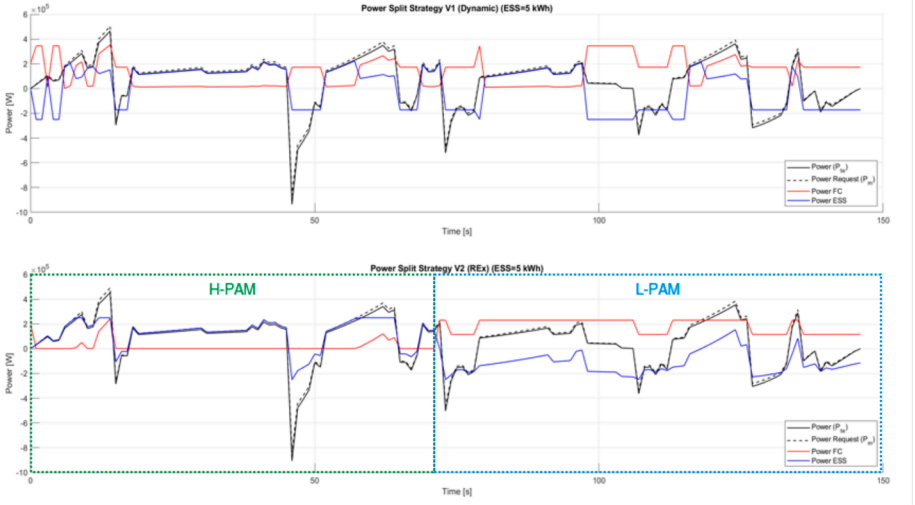

Fig. 6. Power split strategies for FCHEV (Magny-Cours circuit) with ESS = 5 kWh: V1 (top) and V2 (bottom).

the SOC_{REx_up} (or the initial SOC if at the end of the duty cycle) is recovered. This strategy is inspired to the published data for the Hyundai N Vision 74 concept [26], and the powertrain specifications of this concept denote an optimization of the power distribution to ensure performance while simultaneously maintaining a FC power lower than 100 kW. It should be noted that even with this strategy the possibility exists that the FC must deliver all the power required by the drive cycle. This situation could arise when the ESS is in a state of low SOC or if it is undersized, causing the power demand to exceed the limits of discharge power imposed, and in Fig. 5 this value (ESS_{th}) is reported for both the strategies described. In addition, the power recuperated from regenerative braking is indicated as P_{rb}. The section of the code when $P_{te} < 0$ is not reported in the synthetic map of the V2 strategy as it is equal to that of the V1 strategy (Fig. 4).

The graphical representation in Fig. 6 exemplifies the power distribution for a single lap with a 5 kWh ESS, employing the telemetry data from Section 2.2, and it is reported here for methodology explanation purposes. The inherent disparity between V1 and V2 strategies is distinctly observable. Indeed, the former strategy is characterized by a primary FC contribution, with the ESS assuming a supportive role during peak power demands throughout the driving cycle. The second power distribution strategy (V2) in Fig. 6 shows the two power assistance modes (H-PAM and L-PAM) constituting the V2 strategy. As evident, in the H-PAM mode the ESS significantly contributes to the load management. This mode persists until the predefined SOC_{REx_low} limit is attained (as illustrated in the specific case, 71 s from the beginning of the drive cycle). Subsequently, the system shifts to the L-PAM mode, wherein the computation of the target power required to restore the initial SOC is undertaken. In this phase, the ESS partially follows the demanded load while simultaneously is being recharged by the combined FC power delivery and the regenerative braking. Both strategies conform to the aggressive driving style as classified in [27], and in Fig. 6-b two levels of target FC power are distinguishable, corresponding to the target value itself and its half.

2.5. Hydrogen consumption

Regarding hydrogen consumption, the available fuel cell data (e.g. from published datasets, [23]) are used as a benchmark for the current state-of-the-art polarization curve for high-performance fuel cell stacks. These are used to design a representative fuel cell stack model aligning with the power range typical of the load for the examined duty cycle. The fundamental curves representing the fuel cell model performance are depicted in the Fig. 7.

The model is used to derive the data pertaining the operating points of the FC system starting from the requested FC power (Fig. 7-a) to obtain the individual cell voltage and current (Fig. 7-b), finally calculating the associated hydrogen consumption. The code implements the fundamental FC equations based on the Faraday's law to derive the hydrogen flow rate for given current and voltage cell operation, as in Eq. 14 where $\dot{m}_{H2}$ is the hydrogen mass flow rate, P is the FC power, M_{H2} is the molar mass of hydrogen, n_e is the number of exchanged electrons per fuel molecule (equal to 2 for hydrogen), F is the Faraday's constant and V is the cell voltage. The mass of the consumed hydrogen is calculated

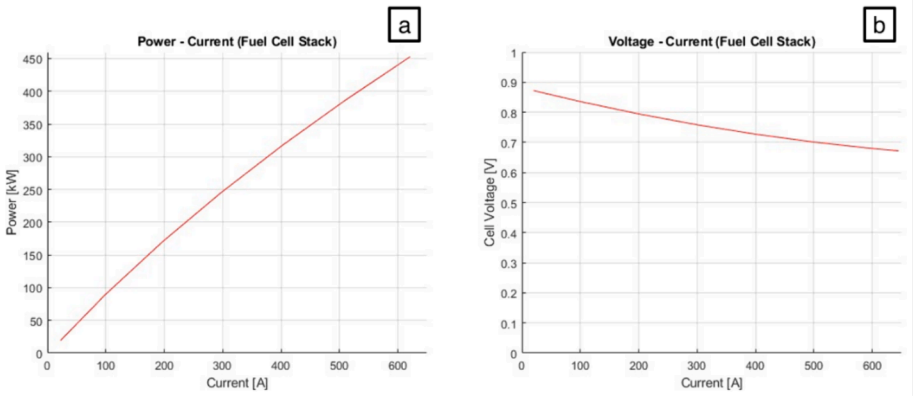

Fig. 7. Power-current (a) and polarization (b) curves for the fuel cell stack model.

Table 2
Vehicle parameters and efficiencies.

Parameter	Value
Vehicle mass, m [kg]	1125
Frontal area, A [m^2]	2
Drag coefficient, C_d	0.35
Rolling resistance, μ_{rr}	0.012
η_g [2]	1.0
η_m [21]	0.9215
η_{ess}	1.0

via time integration of Eq. 12 over the entire duty cycle duration.

$$\dot{m}_{H2} = \frac{PM_{H2}}{n_e FV} \quad 14$$

The developed MATLAB code will be made fully accessible upon request fulfilling the FAIR (Findable, Accessible, Interoperable, Reusable) indications.

3. Results

The analysis conducted in this study focuses on the power- and energy-based sizing of a representative hybrid powertrain electric supercar (FCHES). In this context, a comparative evaluation is conducted, considering a range of ESS energy in-between 5–25 kWh. The MATLAB model described in Section 2 is used to determine the suitable FC power rating for each ESS size, and it is applied to the V1 and V2 strategies. Additionally, the regenerative braking coefficient was evaluated as another variable in the 0–40 % interval. The chosen values are consistent with the current state of the art in hybrid powertrain architectures [2], with specific reference to their application in a typical supercar. All the scenarios adhere to identical boundary conditions (Table 1), and as target distance a 5-laps period of the Magny-Cours circuit is considered, obtained by repeating the reference lap telemetry data and consisting in a total distance of 30.7 km and an overall duration of 682 s. This choice ensures a sufficient driving range for coherent strategy comparability: with the highest energy ESS (25 kWh), the V2 strategy did not allowed the SOC recovery for shorter driving distance. This limitation lies in the need that the specified threshold (SOC_{REx_low}) is reached for L-PAM mode activation, as is the case with ESS $>$ 6 kWh. A shorter mission duration would have prevented the recovery of the initial SOC before the mission end, thus jeopardizing the V2 strategy comparison against V1. Additionally, it is specified that the study requirement for same initial and final SOC is necessary to consider the driving cycle repeatable, thus representing a portion of a hypothetical longer race duration.

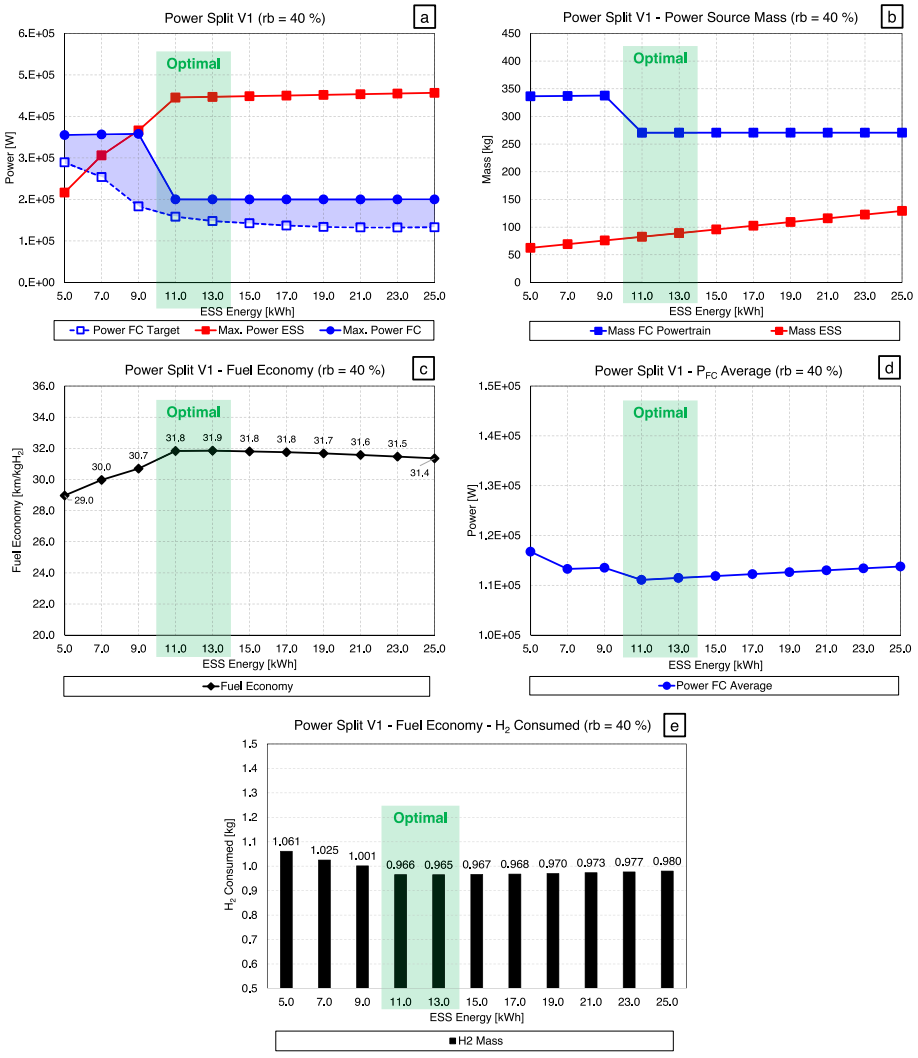

Fig. 8. Results for V1 strategy (rb = 40 %): a) Power split [W] with indication of FC power range in light blue area, b) Power source mass [kg], c) Fuel economy [km/kgH_2], d) Power fuel cell average [W], e) Cumulative H_2 consumption [kg]. ESS data in red, FC data in blue, powertrain data in black. (For interpretation of the references to colour in this figure legend, the reader is referred to the web version of this article.)

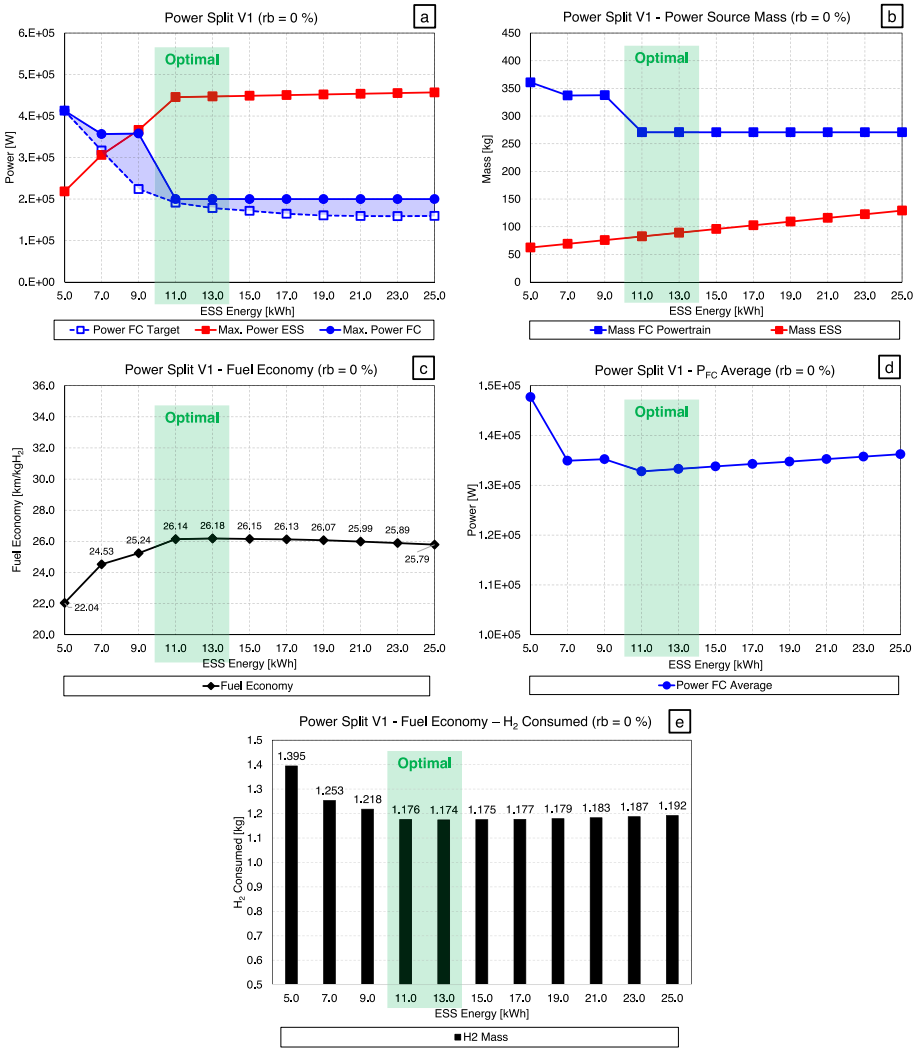

Fig. 9. Results for V1 strategy (rb = 0 %): a) Power split [W] with indication of FC power range in light blue area, b) Power source mass [kg], c) Fuel economy [km/kgH_2], d) Power fuel cell average [W], e) Cumulative H_2 consumption [kg]. ESS data in red, FC data in blue, powertrain data in black. (For interpretation of the references to colour in this figure legend, the reader is referred to the web version of this article.)

For completeness, it is specified that the road elevation of the circuit is ignored, thus the term in Eq. (3) is zero. In Table 2 the used vehicle parameters are reported, including the efficiencies utilized in the model. All the values used for efficiencies in the present study are chosen as the most realistic values to the authors' knowledge, for the sake of results representativeness. Concerning the ESS efficiency (η_{ess}), it is typically in the range of 0.95. However, in this model and for the sake of powertrain comparison, it is assumed as unity in all the analyses, accepting a minor error relatively to the power input/output for the ESS.

Considering the value of η_g, the Eq. (8) results $P_{mot_{out}} = P_{te}$. Equally to what is established for the acceleration phase in the preceding equation, the same simplification is adopted for the deceleration phase (Eq. (9)). The gross weight of the vehicle is obtained by adding the mass of the driver, fuel, and powertrain. In this study, the powertrain architecture of the fuel cell hybrid electric supercar comprises the FC and an ESS, e.g. the battery pack.

3.1. V1 strategy results

Fig. 8 illustrates the results obtained from implementing the model employing the V1 strategy, with a regenerative braking value of 40 %. The upper-left graph (Fig. 8-a) delineates the curves representing the maximum power outputs of both the ESS and the FC, along with its target power. For the sake of clarity, the target power denotes the minimum power which the FC is required to deliver to ensure the restoration of the SOC to its initial condition. As illustrated in the synthetic maps (Fig. 4, Fig. 5), this power is provided by the FC in accordance with the demanded load and the SOC. Furthermore, the maximum power output of the FC is contingent on these conditions and represents the peak power that the FC must provide throughout the drive cycle. The trend (Fig. 8-a) illustrated by the target power shows a reduction for increasing ESS energy, which is the opposite trend than the increasing maximum ESS power, which stabilizes at 11 kWh. This is explainable by considering the FC and ESS complementary role in vehicle propulsion: as the ESS size and energy increase, its supportive role grows in the tractive effort, leaving a reduced power burden on the FC. This trend stabilizes at the peak values required by the driving cycle are achieved, rendering further ESS or FC size increase unnecessary (or even negative, considering the added weight and volume). The increase in the ESS size and its capacity to handle an extended power range adverses the demand on the FC, reducing the number of power level variations it needs to perform during the driving cycle and ultimately lowering the FC power rating itself. The FC mass (Fig. 8-b) clearly follows a trend similar to the maximum FC power delivered during the driving cycle, as lightweight solutions are more and more sufficient to deliver a reduced power [24], and this explains its independence on mass for ESS capacity higher than

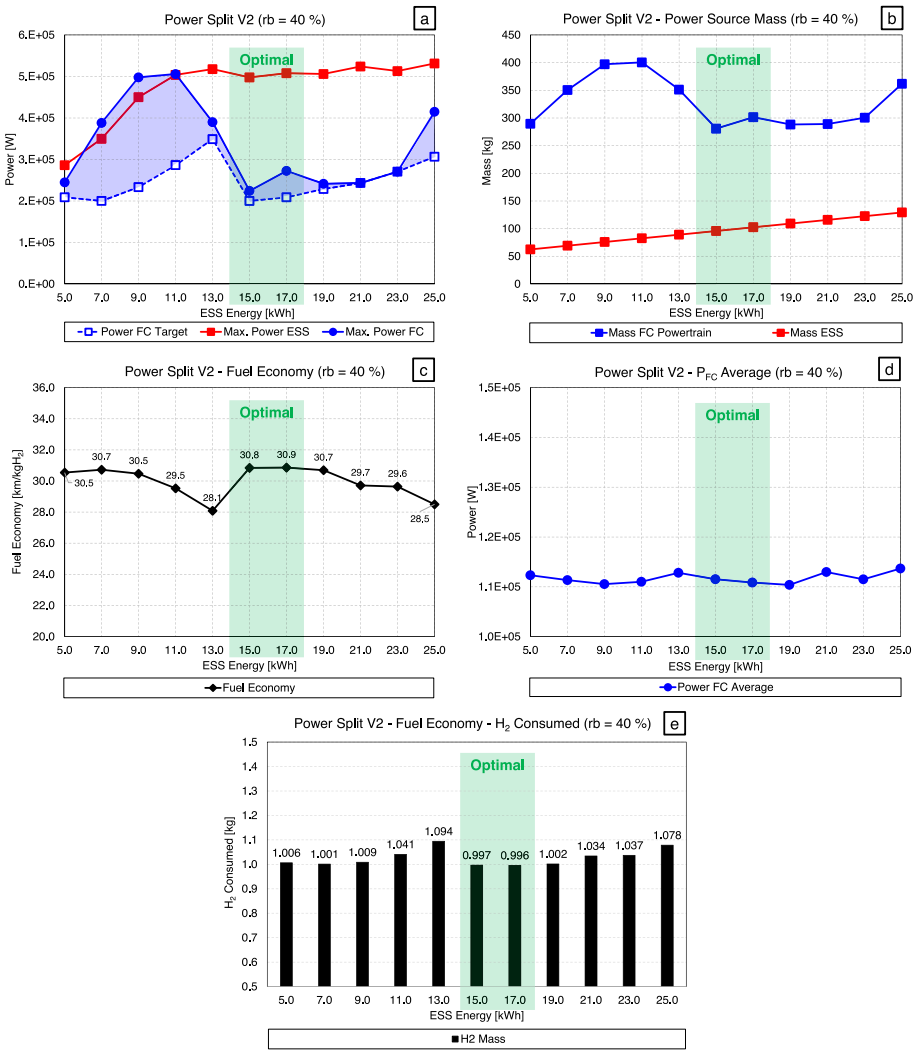

Fig. 10. Results for V2 strategy (rb = 40 %): a) Power split [W] with indication of FC power range in light blue area, b) Power source mass [kg], c) Fuel economy [km/kgH_2], d) Power fuel cell average [W], e) Cumulative H_2 consumption [kg]. ESS data in red, FC data in blue, powertrain data in black. (For interpretation of the references to colour in this figure legend, the reader is referred to the web version of this article.)

11 kWh in Fig. 8-b. On the other hand, the ESS mass increases linearly with the stored energy. Regarding the hydrogen consumption, the data collected in Fig. 8-c/e indicate the optimal solution, here identified in a powertrain configuration with a 13 kWh ESS and 200 kW peak power FC. The examined version demonstrates similar cumulative hydrogen consumption values in the 11–13 kWh versions: however, a slight ESS oversizing to 13 kWh could prove advantageous in terms of lower FC target power at the cost of a moderate weight increase. Subsequently, the trend clearly shows an increase with the growth of the ESS energy and, consequently, its mass, resulting in a deterioration of consumption performance. It is here underlined that despite the oversized configurations show a marginal increase in hydrogen consumption, the small or higher entity of it is considered of secondary relevance in this study, aiming at identifying a reference optimal size of FC and of the battery based on the absolute minimum hydrogen use.

The analysis of the results for the V1 strategy is completed by examining the effects of the absence of regenerative braking on the powertrain architecture, i.e. the ESS recharging is only operated by the FC. The results in Fig. 9 show no substantial differences in terms of power split (a) and power source masses (b) trends. However, the deviation in results is remarkable in hydrogen consumption and the average FC power. Ultimately, similar to the case with 40 % regenerative braking, the optimal solution (highlighted in green) in terms of fuel economy (c, e) is the powertrain configuration utilizing a 13 kWh ESS and a FC with a maximum deliverable power of 200 kW. In this case as well, a close resemblance in hydrogen consumption values is observed with the 11 kWh and 15 kWh powertrain versions, explainable by the same considerations made earlier. The combination of a lower ESS mass compared to the 15 kWh case and lower fuel cell target power compared to the 11 kWh case justifies the 13 kWh version as the superior solution. From this point onward, the increase in hydrogen consumption (e) shows a clear worsening trend.

3.2. V2 strategy results

Moving to V2 strategy, the results for the same span of ESS energy (5–25 kWh) are reported in Fig. 10, with a regenerative braking value of 40 %. Referring to the power split graph (a), a notable differentiation is observed compared to the trends previously outlined for the V1 strategy. Specifically, the trend of the FC target power exhibits a peak at a ESS energy content of 13 kWh, contributing to a non-monotonic pattern. For a clear understanding of this phenomenon, it is necessary to delve into a discussion concerning the SOC.

Fig. 11 illustrates the SOC throughout the entire driving cycle for ESS energy values of 13 and 15 kWh. For a 13 kWh ESS, the model prediction entails discharging from the initial SOC level ($SOC_{REx\_up} = 0.95$) to the

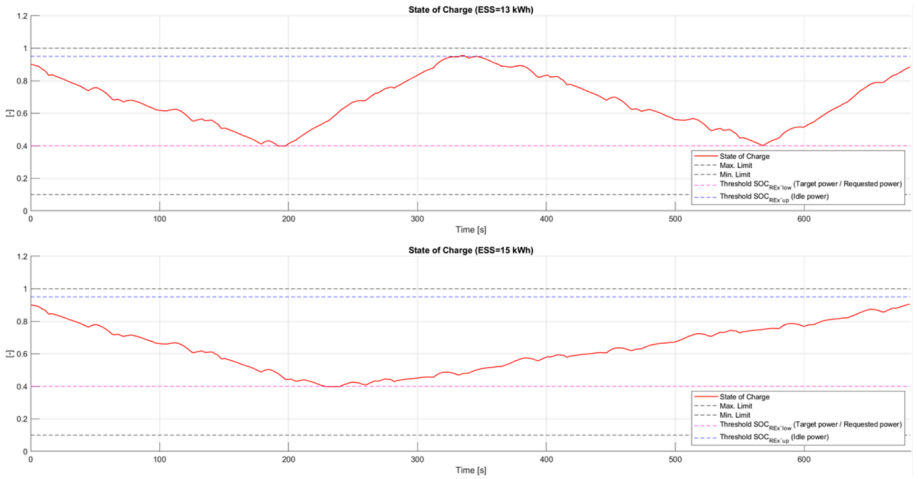

Fig. 11. SOC of the ESS for the V2 strategy: 13 kWh (top), 15 kWh (bottom).

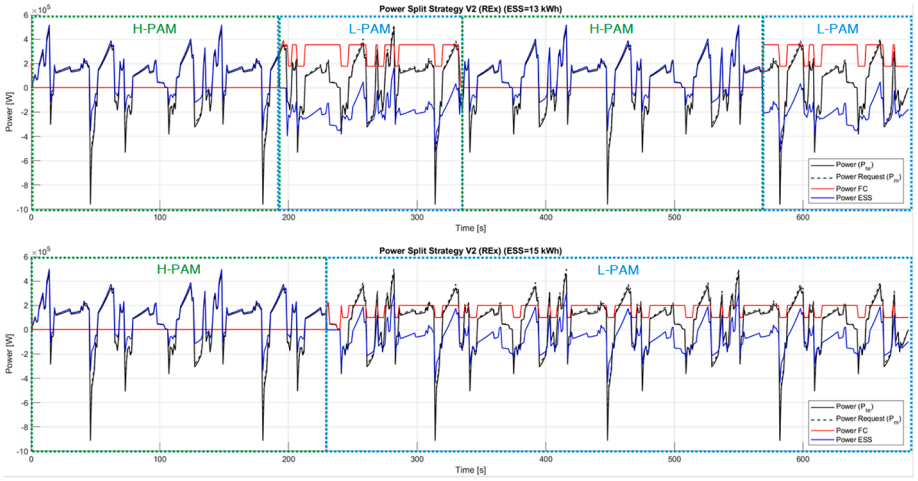

Fig. 12. Power split employing V2 strategy for 5 laps of Magny-Cours circuit for 13 (top), 15 (bottom) kWh ESS.

specified threshold (SOC_{REx_low} = 0.4), followed by a complete recharging phase. This procedure is repeated twice within the duration of 5 laps of the circuit under examination. This pattern is attributed to the insufficiency of the 13 kWh ESS for the specified duty cycle, resulting in two distinct discharge-recharge phases and requiring a more powerful FC. In the powertrain version equipped with a 15 kWh ESS, a single discharge and recharge cycle within the thresholds suffices for the same mission, hence explaining the different trend in Fig. 11.

The highlighted difference significantly impacts the final value of the target power. In Fig. 12, the graphs related to the power split for the 13 and 15 kWh cases are presented. It is notable that, in the case of the 13 kWh, the ESS operates in L-PAM mode twice, each with a duration shorter than 150 s. The target power, as reported in Fig. 10-a, is approximately 354 kW. Conversely, with the 15 kWh ESS, the optimization model manages the FC power flow by significantly extending (>400 s) the duration of the L-PAM mode for the ESS, resulting in a lower target power for the FC to restore the initial SOC. However, it is underlined that such discontinuity in results is clearly due to the specific vehicle and duty cycle, whose occurrence will vary with the variation of any of the model boundary conditions, but which must always be accounted for. Ultimately, the limits imposed by the ESS energy content prove to be disadvantageous in terms of hydrogen consumption, as it implies a higher maximum power that the FC must deliver, and consequently, a higher overall mass of the FC system (351 kg for the 13 kWh ESS, dropping to 281 kg for the 15 kWh ESS). The most efficient solutions (highlighted in green, Fig. 10-e) with the V2 strategy under consideration, in terms of fuel economy, are identified in the versions with a 15 and 17 kWh ESS and a peak FC power respectively of 224 and 272 kW. These versions align with the previously described single charge–discharge cycle pattern for the mission under consideration. The cumulative consumed hydrogen value is very similar even in the case of the 15 kWh ESS, although the slight advantage in lower average power of the FC (d) is crucial despite its worse characteristics in terms of higher maximum power (a) and, therefore, system mass (b).

Finally, the results for power split optimization with the V2 strategy are analysed without regenerative braking, as in Fig. 13. Regarding the FC target power (a), for cases with 9 kWh and 11 kWh, the transition from two to a single discharge-recharge cycle is evident, and the explanation is the same as that observed in the previous paragraph with regenerative braking. As for the maximum FC power, a non-monotonic trend is observed with increasing ESS energy. The variability in this curve is a direct consequence of the power peaks in the drive cycle that must be respected, especially with a low-energy ESS or with a low SOC. The latter case is here particularly critical due to the lack of braking energy recovery, resulting in higher demand on the FC to maintain the SOC above the minimum threshold and restore it to the initial value. The mass trend (b) closely follows the required maximum power. Under the assumptions set for this strategy, the power distribution optimization model highlights the powertrain version with a 7 kWh ESS as the best solution in terms of hydrogen consumption. This aligns with the

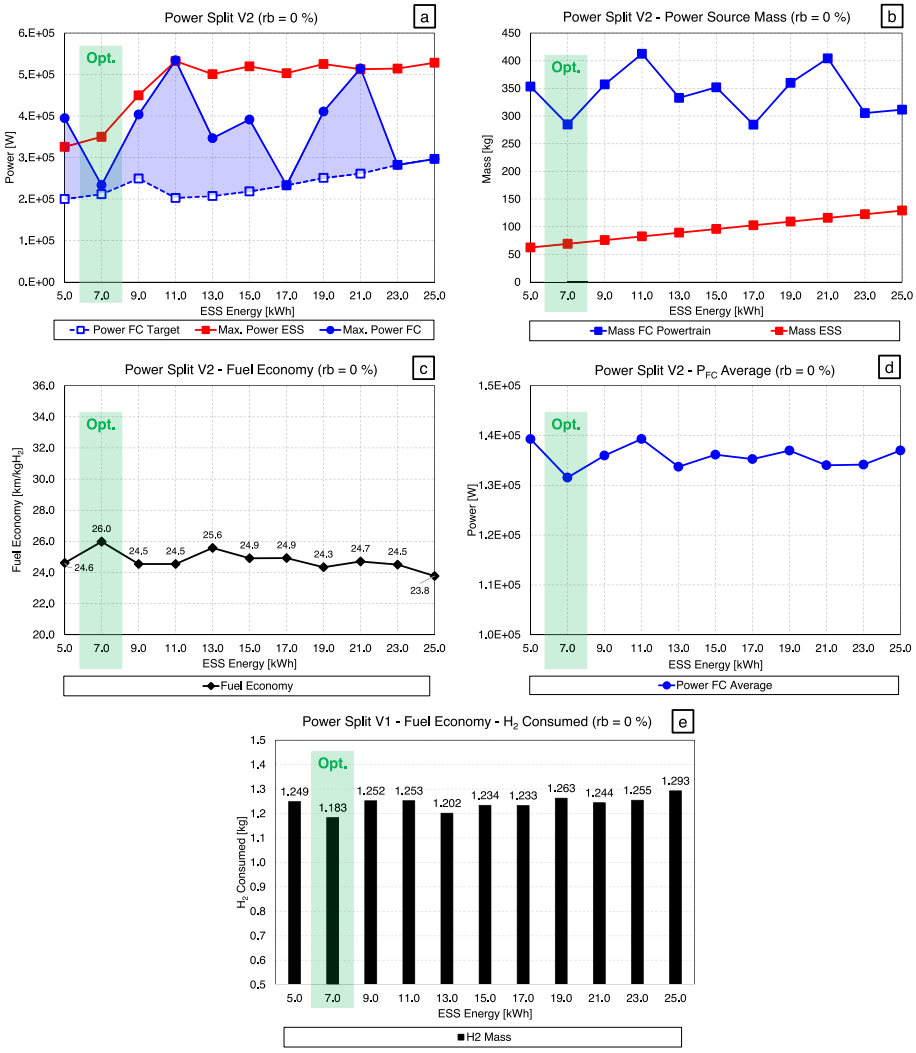

Fig. 13. Results for V2 strategy (rb = 0 %): a) Power split [W] with indication of FC power range in light blue area, b) Power source mass [kg], c) Fuel economy [km/kgH_2], d) Power fuel cell average [W], e) Cumulative H_2 consumption [kg]. ESS data in red, FC data in blue, powertrain data in black. (For interpretation of the references to colour in this figure legend, the reader is referred to the web version of this article.)

principles defining the V2 strategy. Opting for a smaller ESS with a reduced energy content is advantageous, resulting in weight savings. Additionally, less power is required for recharging it to identical thresholds, leading to hydrogen savings. Despite the dual cycle of discharging and charging (Fig. 11), it remains more convenient in terms of fuel economy. In fact, this version is associated with a fuel cell with a peak power of 234 kW, with the lowest fuel cell system mass (285 kg).

3.3. Comparison of best-performing cases

With the aim of globally comparing the four set of results (for V1 and V2 strategy, with and without regenerative braking), in Fig. 14 the best-performing cases concerning fuel economy are reported. The results show that the V1 strategy is advantageous for both regenerative braking values. In terms of FC target power (a), V1 (rb = 40 %) exhibits the lowest fuel consumption values, and likewise, the maximum FC power values for V1 are lower than the V2 counterparts, resulting in a benefit in terms of the total mass of the powertrain (b). As expected, the average power (d) at which the FC must operate to follow the imposed vehicle mission is lower for the V1 strategy by 19.6 % in the comparison between the two regenerative braking coefficient values. The same comparison for the V2 strategy yields a difference of 18.6 %. The disparity between the two strategies, at an equal regenerative braking value, is considerably smaller (<0.15 %). The absence of regeneration contribution results in a significant burden in terms of fuel economy and consumed hydrogen (c, e). As evident, the increase in cumulative hydrogen consumption for completing the mission amounts to +21.6 % and +18.7 %, respectively, for the V1 and V2 strategies. This would imply, in the design phase, considering a higher on-board hydrogen mass and, an increased volume for hydrogen storage; however, this is not considered in the overall mass evaluation given the lower order of magnitude and the negligible impact on the powertrain mass. Ultimately, the V1 strategy performs better than the V2 strategy regarding fuel economy, saving around 3.2 % of hydrogen for the mission of 5 laps of the Magny-Cours circuit.

Additionally, an analysis of the FC power intermittency is conducted, along with the time spent at different power levels during the drive cycle (f), where the number of power variations and duration spent at idling, target and requested power is reported. Specifically, the power requested encompasses all the power values delivered by the FC, excluding those computed as target power. Therefore, it pertains to all power fluctuations imposed by the load that must be supplied by the FC itself, specifically in cases where the required power exceeds the predetermined threshold for the ESS (ESS_{th}) or in case of low SOC. Particularly noteworthy is that the V1 strategy must adjust the power level 175 times, irrespectively of regenerative braking. During the entire drive

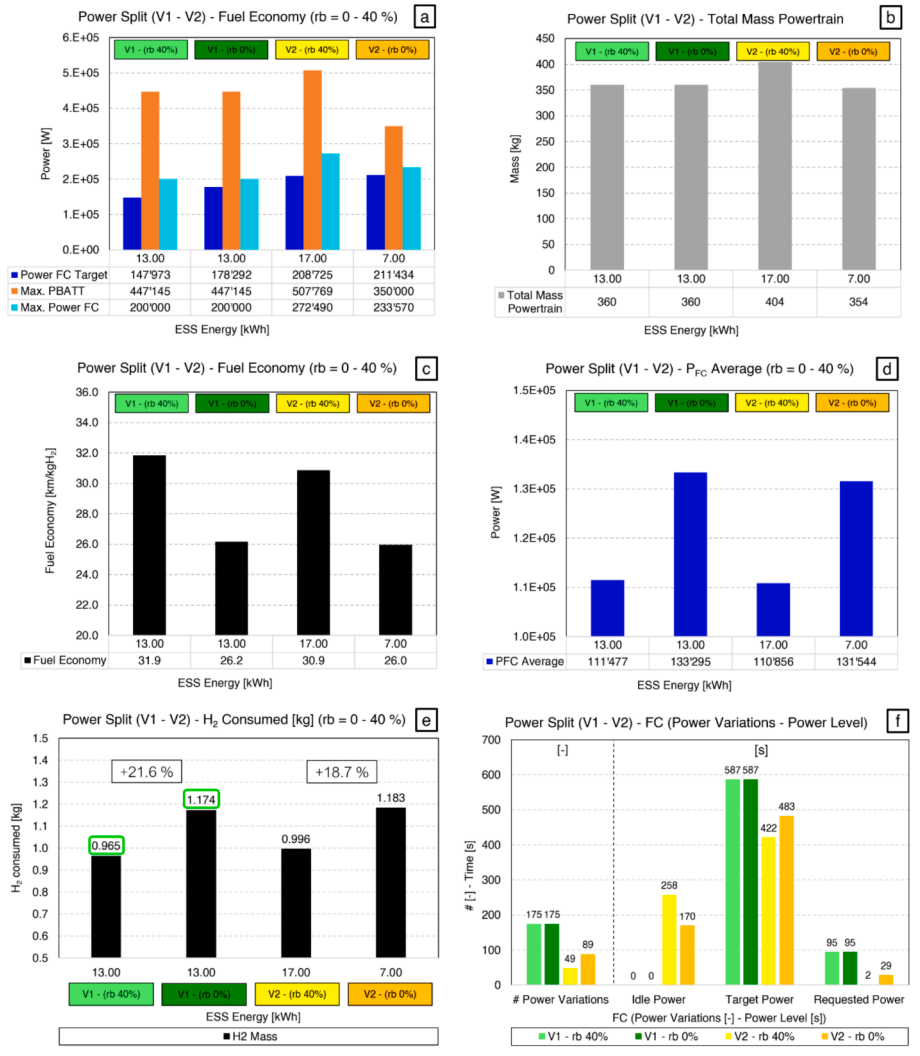

Fig. 14. Results for V1 − V2 strategies (rb = 0–40 %): a) Power split [W], b) Total mass powertrain [kg], c) Fuel economy [km/kgH_2], d) Power fuel cell average [W], e) Cumulative H_2 consumption [kg], f) Fuel cell use (power variations [-], power level [s]).

cycle duration (682 s), 587 s are spent on the value of target power (86 % of the total time), and in the remaining 95 s (14 % of the total time) the FC modulates the output power to follow the drive cycle request. Under the same regenerative braking strategy (40 %), the V2 strategy is characterized by significantly fewer power level changes than in V1, counting only 49 adjustments for this mission (−72 %). Concerning the time allocation in the V2 strategy, the outcomes reveal a significant duration at idle power (258 s, 38 % of the total time), and in the remaining 422 s (62 % of the total time) at target power, with only 2 s on requested power (0.3 % of the total time). In the absence of regenerative braking, the FC spends less time at idle power (170 s, 25 % of the total time), while the durations at target power (483 s, 71 % of the total time) and requested power (29 s, 4 % of the total time) increase accordingly. Considering that the duty cycle variation is one of the responsible factors for accelerated cell degradation [3,28], the V2 strategy clearly outperforms the V1 one on this aspect, although it may not be the primary focus in a FCHES. However, this implication is of primary importance in cases where the Membrane Electrode Assembly (MEA) degradation is critical due to reactants starvation, oxygen and humidity inhomogeneity, and hot spots caused by imperfect cooling [29]. These are situations that can arise with a highly dynamic load for the FC, especially under a wide range of requested power. Finally, it is underlined that the model generally is confirmed by the similar values obtained under all four scenarios in the mean FC power (110–130 kW, with/without regenerative braking, respectively) as visible in Fig. 14(b), whereas a relatively broader spectrum is identified for the ESS energy (7–17 kWh, Fig. 14(a)). These are fundamental key data to design brand-new hybrid powertrains based on FC/ESS, and their robust calculation is the main aim of the developed methodology.

Finally, another key assessment concerns the rated weight of the fuel storage system. Considering the hydrogen mass consumption values in Fig. 14(e) associated with the defined five laps period of the circuit, and in order to maximize the generality of the study, an arbitrary target value for driving range equal to 120 km is defined. However, another significant degree of analysis regards the choice between two different hydrogen storage technologies, i.e. in cryogenic liquid or compressed gaseous form. These are marked by a multiplicity of complementary advantages and disadvantages, generally favouring the compressed gaseous form due to several technical and energetic issues with cryogenic liquefaction. However, the higher hydrogen density allowed by storage in liquid form will be a crucial factor in a future application, especially in high-performance vehicles, where the quest for weight and size reduction is constant. By these remarks and with the support of some specific weight parameters [30], an additional comparison is carried out (Fig. 15) starting from previous cases regarding the weight of the whole tank system.

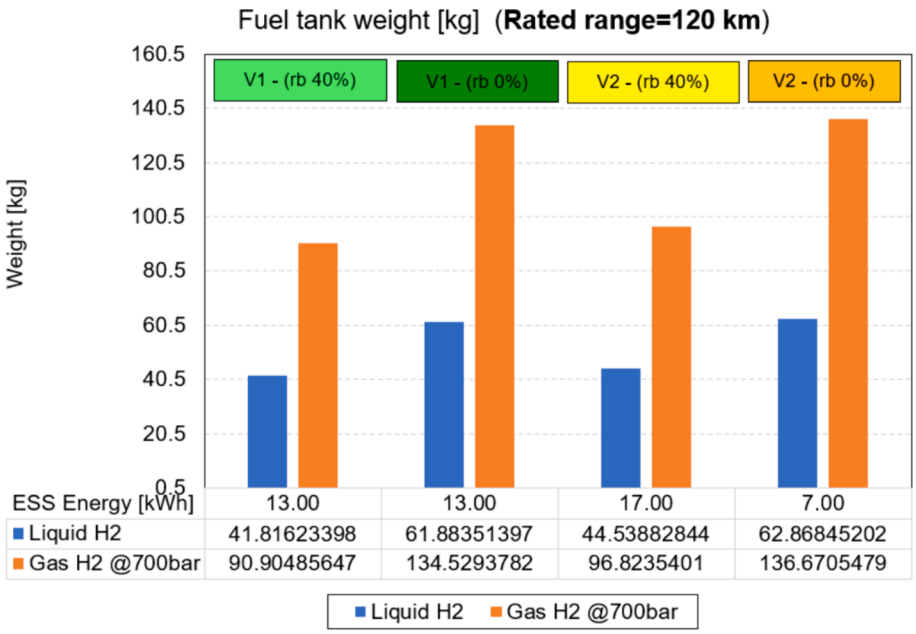

Fig. 15. Results for V1 − V2 strategies (rb = 0–40 %): a comparison between the storage systems weight with the application of two different technologies.

4. Conclusions

In the niche of high-performance applications, the development of Fuel Cell Hybrid Electric Vehicles (FCHEV) assumes a pivotal role as a symbolic representation of disruptive propulsion technology for a sector still reliant on combustion systems (both stand-alone and hybrid). However, defining the power distribution between the main energy sources in a hybrid powertrain is one of the most delicate phases of development, due to the high risk of incurring an undersized or oversized solution, as well as posing severe constraints on virtually all the subsequent design stages. The purpose of this work is to provide a methodology for a rightsized solution by presenting a power split optimization model for a hybrid fuel cell-battery powertrain. Developed in the MATLAB environment and distributed upon request to the authors under the FAIR (Findable, Accessible, Interoperable, Reusable) guidelines, the model considers the drive cycle and the vehicle parameters tailored to the characteristics of typical supercars. In addition, two distinct power split strategies are examined for demonstrating purposes, representing opposing solutions (V1 and V2, i.e. *Dynamic* and *REx*, respectively) each maximizing the utilization of a specific power source. The results indicate that:

- The influence of regenerative braking significantly affects the hydrogen consumption for both operational strategies, leading to a considerable rise in the average FC power and powertrain mass. This ultimately results in an approximate 20 % increase in hydrogen consumption.
- V1 strategy (FC as a primary power source) demonstrates a reduced hydrogen consumption compared to V2, although the difference is marginal, thus reinforcing the methodology generality. Considering that both strategies aim to restore the SOC to its initial state, this highlights how the optimal point in the power distribution is more influenced by the sizing of power/energy of the power sources rather than by the specific strategy.
- V2 strategy (ESS as a primary power source) exhibits significantly reduced utilization of the FC, lowering the frequency of power variations and ensuring an extended life at maximum performance. Although this aspect is not of primary concern in the context of high-performance supercars, it is worth to include it in the analysis for the sake of study generality on different classes of vehicles.
- Both strategies identify an optimal FC peak power in the range of 200 kW (maximum power) and a ESS energy capacity of 11–15 kWh, with the only exception of the V2 (*REx*) strategy without regenerative braking showing an optimal sizing with a smaller (7 kWh) ESS due to the reduced recharging possibility.

The proposed methodology enables the identification of powertrain solutions characterized by primary reference values for power and energy, leveraging the simplicity of a zero-dimension model in providing essential elements to lay the foundations of the project at an early design stage. The power split optimization model ensures a more rapid identification of optimal combinations primarily based on fuel economy, paving the way towards deeper optimization including volume, efficiency, and overall performance of the powertrain.

CRediT authorship contribution statement

Martino Diana: Writing – review & editing, Writing – original draft, Software, Methodology, Data curation, Conceptualization. **Lorenzo Martoccia:** Writing – review & editing, Writing – original draft, Software, Methodology, Data curation, Conceptualization. **Stefano Fontanesi:** Writing – review & editing, Supervision, Funding acquisition, Conceptualization. **Valerio Mangeruga:** Writing – review & editing, Supervision. **Alessandro d'Adamo:** Writing – review & editing, Supervision, Funding acquisition, Data curation, Conceptualization.

Declaration of competing interest

The authors declare that they have no known competing financial interests or personal relationships that could have appeared to influence the work reported in this paper.

Data availability

Data will be made available on request.

Acknowledgements

Martino Diana acknowledges the co-funding provided by FAR (*Fondo Ateneo per la Ricerca*, Dipartimento di Ingegneria "Enzo Ferrari")

Dipartimentale 2022, for the H2CAR project. Lorenzo Martoccia acknowledges the financial support provided by Regione Emilia-Romagna (Italy), Borsa di Dottorato (39 ciclo). Alessandro d'Adamo and Stefano Fontanesi acknowledge the financial support provided by European Union, NextGenerationEU - National Sustainable Mobility Center - MOST, CN00000023, Italian Ministry of University and Research, Spoke 12 (CUP E93C22001070001).

References

[1] Ehsani Mehrdad, Gao Yimin, Longo Stefano, and Ebrahimi Kambiz, "Modern Electric, Hybrid Electric, and Fuel Cell Vehicles," *Modern Electric, Hybrid Electric, and Fuel Cell Vehicles, Third Edition*, Feb. 2018, doi: 10.1201/9780429504884.
[2] James. Larminie and J. Lowry, "Electric vehicle technology explained," p. 342, 2012, Accessed: Sep. 30, 2022. [Online]. Available: https://www.wiley.com/en-us/Electric+Vehicle+Technology+Explained%2C+2nd+Edition-p-9781119942733.
[3] Karpenko-Jereb L, Sternig C, Fink C, Tatschl R. Membrane degradation model for 3D CFD analysis of fuel cell performance as a function of time. Int J Hydrogen Energy 2016;41(31):13644–56. https://doi.org/10.1016/J.IJHYDENE.2016.05.229.
[4] Wipke K, *et al.*, "Advisor 2.0: A Second-Generation Advanced Vehicle Simulator for Systems Analysis," 1999, Accessed: Aug. 03, 2023. [Online]. Available: http://www.doe.gov/bridge/home.html.
[5] Wipke KB, Cuddy MR, Burch SD. ADVISOR 2.1: a user-friendly advanced powertrain simulation using a combined backward/forward approach. IEEE Trans Veh Technol 1999;48(6):1751–61. https://doi.org/10.1109/25.806767.
[6] Markel T, et al. ADVISOR: a systems analysis tool for advanced vehicle modeling. J Power Sources 2002;110(2):255–66. https://doi.org/10.1016/S0378-7753(02)00189-1.
[7] Williamson SS, Emadi A. Comparative assessment of hybrid electric and fuel cell vehicles based on comprehensive well-to-wheels efficiency analysis. IEEE Trans Veh Technol 2005;54(3):856–62. https://doi.org/10.1109/TVT.2005.847444.
[8] Maxoulis CN, Tsinoglou DN, Koltsakis GC. Modeling of automotive fuel cell operation in driving cycles. Energy Convers Manag 2004;45(4):559–73. https://doi.org/10.1016/S0196-8904(03)00176-6.
[9] Senger RD, Merkle MA, Nelson DJ. Validation of ADVISOR as a simulation tool for a series hybrid electric vehicle. SAE Technical Papers 1998. https://doi.org/10.4271/981133.
[10] Kelly KJ, Zolot M, Glinsky G, Hieronymus A. Test results and modeling of the Honda insight using ADVISOR. SAE Technical Papers 2001. https://doi.org/10.4271/2001-01-2537.
[11] Huang M, et al. Research on hybrid ratio of fuel cell hybrid vehicle based on ADVISOR. Int J Hydrogen Energy 2016;41(36):16282–6. https://doi.org/10.1016/J.IJHYDENE.2016.05.130.
[12] Feng L, Chang TC, Weiwei G, Xie YC, Zheng LP. Optimal system parameters and hybrid ratio for fuel cell hybrid electric vehicles. Sens Mater 2020;32(5):1593–607. https://doi.org/10.18494/SAM.2020.2694.
[13] Cipollone R, Di Battista D, Marchionni M, Villante C. Model based design and optimization of a fuel cell electric vehicle. Energy Procedia 2014;45:71–80. https://doi.org/10.1016/J.EGYPRO.2014.01.009.
[14] Di Battista D, Villante C, Cipollone R. Optimal components design of a fuel cell electric vehicle. SAE Technical Papers 2015;2015(September). https://doi.org/10.4271/2015-24-2546.
[15] Carignano M, Costa-Castello R. Toyota Mirai: Powertrain model and assessment of the energy management. IEEE Trans Veh Technol 2023. https://doi.org/10.1109/TVT.2023.3237173.
[16] Di Ilio G, Di Giorgio P, Tribioli L, Bella G, Jannelli E. Preliminary design of a fuel cell/battery hybrid powertrain for a heavy-duty yard truck for port logistics. Energy Convers Manage 2021;243:114423. https://doi.org/10.1016/J.ENCONMAN.2021.114423.
[17] Jouda B, Jobran Al-Mahasneh A, Mallouh MA. Deep stochastic reinforcement learning-based energy management strategy for fuel cell hybrid electric vehicles. Energy Convers Manage 2024;301:117973. https://doi.org/10.1016/J.ENCONMAN.2023.117973.
[18] Li M, Wang Y, Yu P, Sun Z, Chen Z. Online adaptive energy management strategy for fuel cell hybrid vehicles based on improved cluster and regression learner. Energy Convers Manage 2023;292:117388. https://doi.org/10.1016/J.ENCONMAN.2023.117388.
[19] Hu H, Yuan WW, Su M, Ou K. Optimizing fuel economy and durability of hybrid fuel cell electric vehicles using deep reinforcement learning-based energy management systems. Energy Convers Manage 2023;291:117288. https://doi.org/10.1016/J.ENCONMAN.2023.117288.
[20] Fu H, Yang D, Wang S, Wang L, Wang D. A novel online energy management strategy for fuel cell vehicles based on improved random forest regression in multi road modes. Energy Convers Manage 2024;305:118261. https://doi.org/10.1016/J.ENCONMAN.2024.118261.
[21] Asus Z, Aglzim E-H, Chrenko D, Daud Z-H-C, Le Moyne L. Dynamic modeling and driving cycle prediction for a racing series hybrid car. IEEE J Emerg Sel Top Power Electron 2014;2(3):541–51. https://doi.org/10.1109/JESTPE.2014.2307079.
[22] Onori S, Serrao L, Rizzoni G. Hybrid electric vehicles: energy management strategies. SpringerBriefs Control Automation Robot 2016;(9781447167792):1–112. https://doi.org/10.1007/978-1-4471-6781-5/COVER.
[23] "https://www.ballard.com/docs/default-source/spec-sheets/fcgen-hps.pdf?sfvrsn=704ddd80_6".
[24] "https://www.batterydesign.net".
[25] Warner J. "The handbook of lithium-ion battery pack design: Chemistry, components, types and terminology," *The Handbook of Lithium-Ion Battery Pack Design: Chemistry, Components, Types and Terminology*, pp. 1–239, May 2015, doi: 10.1016/C2013-0-23144-5.
[26] "https://www.hyundai-n.com/en/models/rolling-lab/n-vision-74.do".
[27] Langari R, Won JS. Intelligent energy management agent for a parallel hybrid vehicle - Part I: system architecture and design of the driving situation identification process. IEEE Trans Veh Technol 2005;54(3):925–34. https://doi.org/10.1109/TVT.2005.844685.
[28] Wu J, et al. A review of PEM fuel cell durability: degradation mechanisms and mitigation strategies. J Power Sources 2008;184(1):104–19. https://doi.org/10.1016/J.JPOWSOUR.2008.06.006.
[29] F. Barbir, "PEM fuel cells: theory and practice," p. 518, 2013.
[30] Cheng Q, Zhang R, Shi Z, Lin J. Review of common hydrogen storage tanks and current manufacturing methods for aluminium alloy tank liners. Int J Lightweight Mater Manuf 2024;7(2):269–84. https://doi.org/10.1016/J.IJLMM.2023.08.002.